Characterization of Stationary and Nonstationary Behavior in Gyrotron Oscillators

T. H. Chang,[1] S. H. Chen,[2] L. R. Barnett,[1] and K. R. Chu[1]
[1]*Department of Physics, National Tsing Hua University, Hsinchu, Taiwan*
[2]*National Center for High-Performance Computing, Hsinchu, Taiwan*
(Received 20 April 2001; published 18 July 2001)

The transition from the stationary state to a sequence of nonstationary states in the gyromonotron oscillator is experimentally characterized for the first time. We have also demonstrated the *stationary* operation of a gyrotron backward-wave oscillator at a beam current far in excess of the generally predicted nonstationary threshold. This difference in nonlinear behavior has been investigated and shown to be fundamental with a comparative analysis of the feedback mechanisms, energy deposition profiles, and field shaping processes involved in these two types of oscillations.

DOI: 10.1103/PhysRevLett.87.064802 PACS numbers: 84.40.Ik, 84.40.Fe

The gyrotron is a coherent radiation source based on the electron cyclotron maser interaction. In the oscillator version, the gyromonotron provides the highest average millimeter-wave power to date for such applications as fusion plasma heating, while the gyrotron backward-wave oscillator (gyro-BWO), though much less developed, features continuous frequency tunability. Inherently a high power source, the gyrotron is susceptible to a variety of single-mode and multimode nonstationary behavior. In various ways, it imposes severe limitations on the performance of the gyrotron. Here, we study the nonstationary behavior resulting from the overdrive of a single mode in the gyrotron oscillator. The threshold current of a single-mode nonstationary state reported thus far [1–7] is typically several times higher than the start-oscillation current. Immediately above the threshold, the field energy bounces back and forth between the ends of the interaction structure, which modulates the local amplitude of oscillation (hence, generates sidebands) at a frequency approximately given by

$$\Delta f = 1/2\tau, \tag{1}$$

where τ is the wave transit time from end to end at the group velocity [1,2,4,6]. As the beam current increases further, the system transitions from such a self-modulation state into a chaotic state [2–5]. During the transition, doubling of the modulation period was observed in a simulation study [4].

In a recent theoretical study [8] of the gyro-BWO, however, it was shown that the axial field profile contracts in the nonlinear regime which therefore suggests the possibility of stationary (saturated) operation at a beam current as high as 2 orders of magnitude above the self-modulation threshold predicted by early theories. Because Ref. [8] employed a stationary code, no direct verification of this possibility was given.

In this paper, we present the first experimental verification and characterization of such sharply contrasting nonlinear behaviors as well as an analytical examination of the underlying physics. The geometry and dimensions of the Ka-band interaction structure under study are identically shown in Figs. 1b and 2b for two regimes of operation (Figs. 1a and 2a). In the gyromonotron regime and gyro-BWO regime, the beam line intersects, respectively, with the forward branch and backward branch of the TE_{11} mode. The primary interaction section, 10 cm in length and uniform in cross section, is connected at each end by a 5 cm up-taper to a uniform output section 0.7 cm in length. The two identical tapers, with a 0.57° taper angle

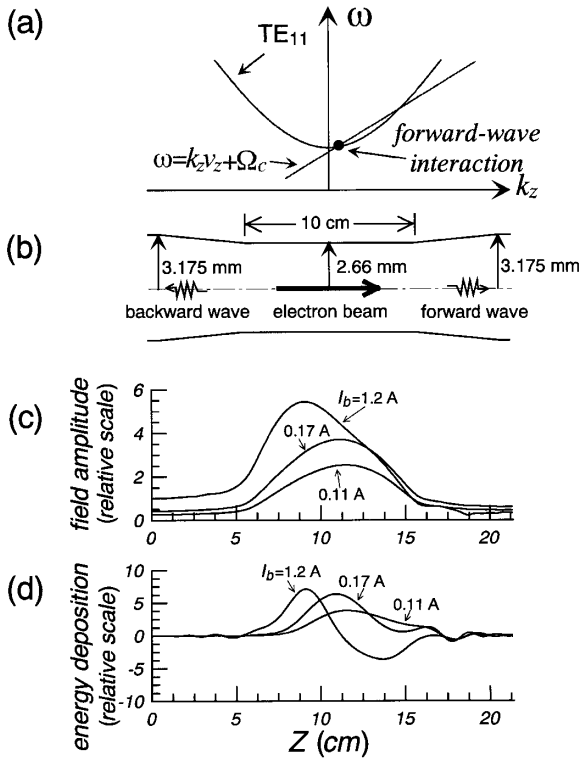

FIG. 1. (a) Operating point of the gyromonotron in the $\omega - k_z$ diagram. Ω_c is the electron cyclotron frequency. (b) Geometry and dimensions of the interaction structure. Beam generated waves are shown to emerge from both open ends. (c) Calculated linear and nonlinear field profiles for $V_b = 100$ kV, $\alpha = 1$, $r_c = 0.09$ cm, and $B_0 = 13.47$ kG. A cold beam was assumed. (d) Calculated beam energy deposition profiles in the corresponding fields shown in (c).

 0031-9007/01/87(6)/064802(4)$15.00

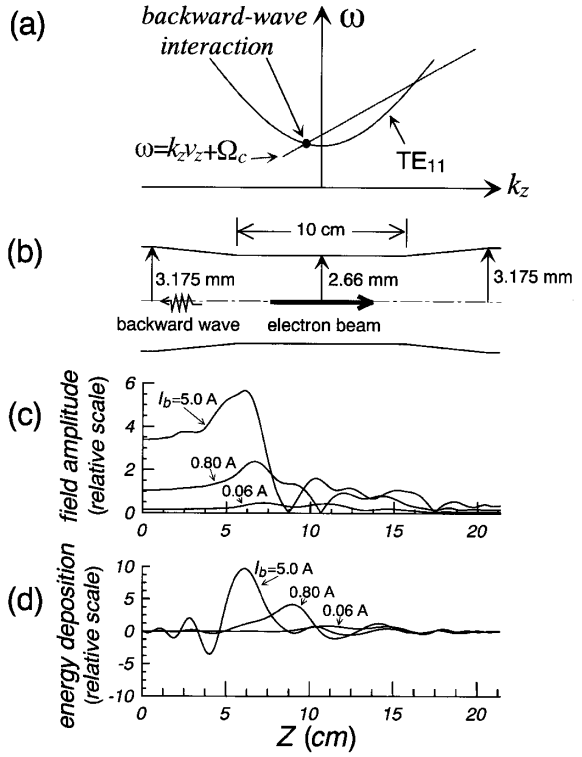

FIG. 2. (a) Operating point of the gyro-BWO in the $\omega - k_z$ diagram. (b) Same interaction structure as in Fig. 1a, showing the beam generated wave coming out predominantly from the upstream end. (c) Calculated linear and nonlinear field profiles for $V_b = 100$ kV, $\alpha = 1$, $r_c = 0.09$ cm, and $B_0 = 14.59$ kG. A cold beam was assumed. (d) Calculated beam energy deposition profiles in the corresponding fields shown in (c).

and slightly elongated cross section, function as converters between circularly and linearly polarized waves [9,10]. Less abrupt electron bunching in the upstream taper also enhances the interaction efficiency. The measured conversion loss was only ~0.2 dB. A 100 kV annular electron beam, generated by a magnetron injection gun, was used in the experiment. Simulated electron trajectories show equal perpendicular and parallel velocities ($\alpha = 1$) with guiding centers located at the radial position (r_c) of 0.09 cm. The applied magnetic field (B_0), provided by a superconducting magnet, is uniform throughout the structure.

A particular feature of the experiment is that we employ the same setup for both gyromonotron and gyro-BWO studies. The transition from one regime to the other was effected by magnetic field adjustment only. It is therefore possible to make a direct comparison of measured effects and quantities between these two types of oscillations.

For the theoretical analysis, a single (TE_{11}) mode was assumed. The set of wave and electron dynamics equations [11] were numerically integrated from the left end to the right end under the assumption of a stationary state. Weak reflections from structure nonuniformities as well as mode conversion in the tapers were also modeled. Outgoing-wave boundary conditions have been imposed at both ends, which yield the oscillation frequency as an eigenvalue.

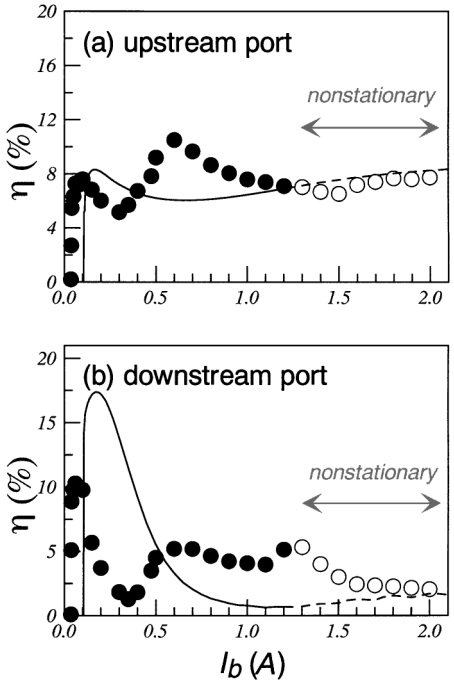

FIG. 3. Measured (dots and circles) and calculated (lines) interaction efficiency (output power divided by beam power) of the gyromonotron at (a) the upstream port and (b) the downstream port as a function of the beam current. Parameters are the same as in Fig. 1.

In the experiment, beam generated waves were coupled out through the side walls of the uniform sections at both ends. Output power was measured with a calibrated crystal detector with estimated accuracy of ±5%. Figures 3a and 3b show the simultaneously measured stationary-state efficiencies (dots) and nonstationary-state averaged efficiencies (circles) of the output powers at, respectively, the upstream and downstream ports of the gyromonotron as functions of the beam current (I_b). Fig. 4 shows the measured stationary-state efficiency (dots) at the upstream port of the gyro-BWO up to $I_b =$ A. No data were taken

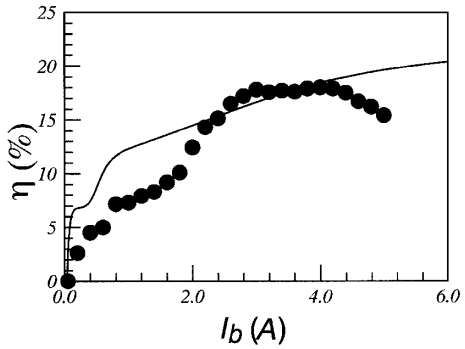

FIG. 4. Measured (dots) and calculated (line) interaction efficiency of the gyro-BWO at the upstream port as a function of the beam current. The detected and calculated power at the downstream port (not shown) was negligible by comparison. Operation was stable at all operating currents. Parameters are the same as in Fig. 2.

for $I_b > 5$ A because of the emergence of coupler oscillations. Downstream port output power of the gyro-BWO (not shown in Fig. 4) was negligible compared to that from the upstream port. Calculated values are also plotted for comparison. The calculation was performed with a stationary code; hence, calculated results are indicated by dashed lines in the nonstationary regime of operation. For both the gyromonotron and gyro-BWO, stationary oscillations were observed to start at $I_b \approx 50$ mA. However, the gyromonotron became nonstationary at $I_b = 1.29$ A, while the gyro-BWO remained stationary up to the maximum operating current of 5 A.

Figures 3 and 4 also reveal an interesting contrast between the feedback mechanisms involved in the oscillations. Feedback in the gyromonotron is externally provided by end reflections; hence, the feedback loop consists of two counterstreaming waves. However, the feedback loop in the gyro-BWO is completely internal, where the forward moving electron beam and the beam generated backward-wave form the round-trip path. The reflective feedback loop at work in the gyromonotron is evidenced by the comparable output power levels (Fig. 3) measured at the upstream and downstream ports, while the predominance of the output power (Fig. 4) at the upstream port of the gyro-BWO is a clear consequence of an internal feedback.

Calculated stationary field profiles of the gyromonotron are shown in Fig. 1c. These profiles represent a stable balance between two processes: the (axially) uneven deposition of the beam energy and the redistribution of the deposited energy at the group velocity of the forward and backward waves present in the cavity. The two curves in Fig. 1d marked by $I_b = 0.11$ and 0.17 A show the beam energy deposition profiles in the linear and saturated states, respectively. The curve marked by $I_b = 1.2$ A shows the deposition profile just prior to the onset of the (experimentally measured) nonstationary state. In the marginally stationary state ($I_b = 1.2$ A), it is seen that the overbunched electron beam rapidly releases its energy to the field, then immediately retrieves a large fraction of it as it propagates downstream. As a result, there is a region of field energy surge, followed by a region of rapid energy depletion. The system is thus on the verge of an energy imbalance. It quickly becomes nonstationary upon further increase in beam current.

Nonstationary behavior was examined with an oscilloscope and a spectrum analyzer (HP8564E). The video response of the detector and oscilloscope is ~260 MHz at 3 dB. The spectrum analyzer is gated with a pin switch to block the rise and fall portions of the signal and, hence, the transient effects. The excellent pulse-to-pulse reproducibility of the output signal allowed adequate resolution at a 30 Hz repetition rate. Figures 5a–5f show the gated signal traces and corresponding spectrograms of the gyromonotron output pulse at different beam currents. The oscillation was stationary, characterized in Fig. 5a, at beam current up to 1.29 A. At $I_b = 1.29$ A, sidebands

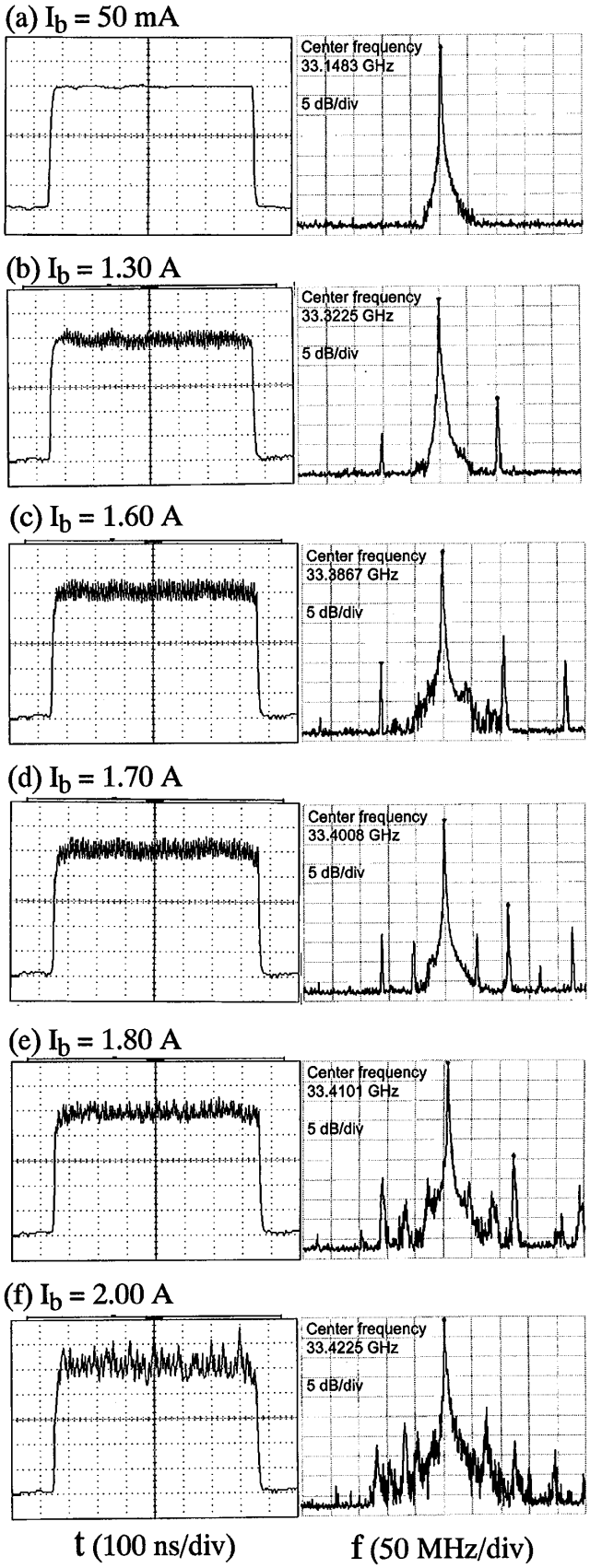

FIG. 5. Signal traces and corresponding spectrograms of the gated gyromonotron output at different beam currents. $V_b = 100$ kV and $B_0 = 13.47$ kG. Transient effects during the raise and fall portions of the pulse had been gated out.

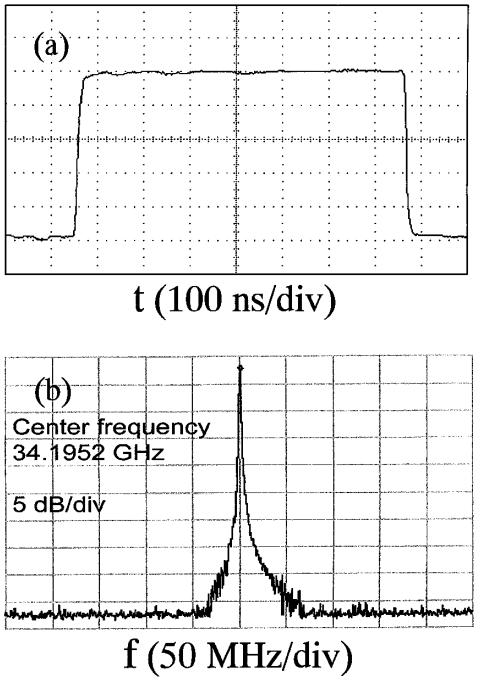

FIG. 6. Stationary signal trace and corresponding spectrogram of the gated gyro-BWO output at a beam current of 5 A (100 times the start oscillation value). $V_b = 100$ kV and $B_0 = 14.59$ kG.

began to appear (Fig. 5b) which are symmetrically separated from the center frequency by approximately 102 MHz, in good agreement with Eq. (1) by assuming an effective interaction length of 18 cm. Harmonic sidebands then emerged at increased beam current (Fig. 5c). Interestingly, at still higher beam currents, doubling (Fig. 5d) and tripling (Fig. 5e) of the modulation period were observed before the oscillation turned stochastic (Fig. 5f). By comparison, even at the maximum operating current of 5 A, the gyro-BWO remained stationary (Fig. 6a) with a spectrum (Fig. 6b) characterized by a single frequency at 34.19 GHz and a spectral width ($\sim$1.2 MHz) consistent with its pulse length.

The dramatically different nonlinear behaviors of the gyromonotron and the gyro-BWO as seen in Fig. 3–6, can be attributed to the basic difference between the two types of feedback mechanisms. Reflective feedback in the gyromonotron results in the formation of a resonant mode whose field profile is shaped primarily by the physical structure rather than by beam-wave interactions. Hence, as shown in Fig. 1c, the linear and nonlinear field profiles differ only in amplitude but maintain essentially the same shape (up to saturation). However, the opposite is true for the gyro-BWO, where the feedback loop does not depend on end reflections. Thus, as first pointed out in Ref. [8] and shown here in Figs. 2c and 2d, more rapid energy depletion at higher beam currents results in increasingly contracted feedback loops and eventually the concentration of the field energy near the upstream end. The much reduced axial extent of the nonlinear field facilitates the energy equilibration required to maintain a stationary state and therefore explains the much higher stationary operating current as well as the much greater saturated output power. It is interesting to note that the observed stationary operating range of the gyro-BWO (Fig. 4) is much broader relative to the conventional BWO for which the reported theoretical [1,6] and experimental [2] nonstationary thresholds are typically 2.5–3.5 times the start-oscillation current. The current study raises the possibility that the nonlinear field contraction in the gyro-BWO might in some way also occur in the conventional BWO, a device with a similar internal feedback circuit.

In summary, we have presented the experimental characterization and theoretical interpretation of the nonstationary behavior of the gyromonotron as well as the much broader stationary operating range of the gyro-BWO resulting from the self-adjustment of the feedback path length. The gyro-BWO is the only continuously tunable and the least exploited version of the gyrotron whose potential is yet to be fully realized. Results of the current study are expected to impact significantly on the power scaling and performance optimization of this class of devices.

This work was supported by the National Science Council, Taiwan. The authors are grateful to Professor N. C. Luhmann, Jr. and Dr. G. S. Nusinovitch for many stimulating discussions and to Dr. J. D. Wang for his technical support.

[1] N. S. Ginzburg, S. P. Kuznetsov, and T. N. Fedoseeva, Izv. Vyssh. Uchebn. Zaved. Radiofiz. **21**, 1037 (1978) [Radiophys. Quantum Electron. **21**, 728 (1978)].
[2] B. P. Bezruchko and S. P. Kuznetsov, Izv. Vyssh. Uchebn. Zaved. Radiofiz. **21**, 1053 (1978) [Radiophys. Quantum Electron. **21**, 739 (1978)].
[3] N. S. Ginzburg, G. S. Nusinovich, and N. A. Zavolsky, Int. J. Electron. **61**, 881 (1986).
[4] A. T. Lin, Z. H. Yang, and K. R. Chu, IEEE Trans. Plasma Sci. **16**, 129 (1988).
[5] A. Y. Dmitriev, D. I. Trubetsko, and A. P. Chtverikov, Izv. Vyssh. Uchebn. Zaved. Radiofiz. **34**, 595 (1991) [Radiophys. Quantum Electron. **34**, 502 (1991)].
[6] B. Levush, T. M. Antonsen, A. Bromborsky, W. R. Lou, and Y. Carmel, IEEE Trans. Plasma Sci. **20**, 263 (1992).
[7] G. S. Nusinovich, IEEE Trans. Plasma Sci. **27**, 313 (1999).
[8] S. H. Chen, K. R. Chu, and T. H. Chang, Phys. Rev. Lett. **85**, 2633 (2000).
[9] L. R. Barnett, L. H. Chang, H. Y. Chen, K. R. Chu, W. K. Lau, and C. C. Tu, Phys. Rev. Lett. **63**, 1062 (1989).
[10] T. H. Chang, L. R. Barnett, K. R. Chu, F. Tai, and C. L. Hsu, Rev. Sci. Instrum. **70**, 1530 (1999).
[11] K. R. Chu, H. Y. Chen, C. L. Hung, T. H. Chang, L. R. Barnett, S. H. Chen, T. T. Yang, and D. J. Dialetis, IEEE Trans. Plasma Sci. **27**, 391 (1999).